Chapter 17

Wideband Wireless Power Transmission to Enhance Efficiency for Low Input Power for Biomedical Applications

Chin-Lung Yang, Yu-Lin Yang and Chun-Chih Lo

Additional information is available at the end of the chapter

http://dx.doi.org/10.5772/46120

1. Introduction

In this chapter, a novel Ultra wideband (UWB) technology is applied in a special aspect for the wireless power transmission (WPT) to achieve a novel wireless wideband powering approach and enhance the power conversion efficiency (PCE) for low average input power. Due to the fact that low transmission power has relatively little impacts and causes relatively slight injury to human bodies, it is one of the essential key technologies in biomedical implant chips and devices. The whole wideband wireless power transmitting and receiving systems are implemented to validate the feasibility of the wireless power transmission system using impulsive waves (wideband power) and the improvement of the conversion efficiency of the rectifier circuitry. This chapter further applies UWB technologies in a special aspect for the transmission of energy rather than messages to achieve a novel wireless impulsive powering approach and enhance the power conversion efficiency for low average input power. The whole impulsive wireless power transmitting and receiving systems are implemented to validate the feasibility of the wireless power transmission using impulsive waves and the improvement of the conversion efficiency of the rectifier circuitry.

UWB technology is important in modern communications systems. Because these devices generally operate in the sub-nanosecond range, designing impulse generator circuitry is particularly challenging. UWB technology has the advantages of low power operation, high data transfer rates, and excellent spatial capacity, making it highly suitable for use in short distance commercial communication systems [Hirt 2003], wireless personal area networks (WPANs), secure communications in military applications, the detection of unexploded ordnance (UXO) and mines, ground penetrating radar (GPR), precision positioning and

tracking [Bertoni 1992], collision avoidance for motor vehicles [Hirt 2003], and innovative wireless power transmission applications as presented in this chapter (Yang 2011).

The idea of wireless power transmission was proposed early in 1899 by Nikola Tesla, and William C. Brown demonstrated the microwave-powered helicopter successfully in 1964 [Brown 1965]. Recently, Intel Corporation fulfilled a high power of wireless coupling to power up electrical appliances, 60-Watt bulbs, with the efficiency more than 75% at the distance of 2 meters in 2008. These show the feasibility of the wireless power transmission technologies. Recently, advanced fabrication techniques of the required components such as rectifiers have enabled a reduction in cost and size that has enabled Radio Frequency Identification (RFID) tags. There are two primary means of wirelessly powering transmission depending on whether the power coupling is through the electric or magnetic field. Inductive coupling of the magnetic field has been used broadly in a great many applications in short ranges [Zimmerman 2006] as well as at high efficiency by resonant magnetic coupling [Kurs 2007]. This sort of the techniques is, however, limited by the distance and the size of the coils. The other method, which most combines with antenna, so-called rectenna, couples power via RF electric fields propagating between high gain external and internal antennas. One attractive feature is that using electromagnetic RF wave propagation for wireless power transmission allows the achievement of a smaller scale in a further operating distance. These rectennas can be formed of any kind of antenna such as dipoles, monopoles, Yagi-Uda antennas, microstrip antennas, spiral antennas, parabolic antenna, retrodirective antennas, and even an antenna array [Rodenbeck 2004]. Also, the rectifier can be implemented by a shunt full-wave rectifier, a bridge rectifier, a voltage doubler, and hybrid types.

Recently, WPT technology has become one of the most-growing, high-impact technologies that will revolutionize the world in the recent years. One of the highlight applications can be useful for biomedical devices. The power supply module for biomedical implantable devices is the core technology among them. Conventionally, batteries or wired power transfer will cause the limitations of implanted devices in time and in space; therefore, the wireless power technology applying in biomedical implantable devices will become an urgent matter and an on-going trend. The most critical part of the wireless power transfer technology is its PCE. To develop an efficient wireless power supply system will prolong to expand the applicable scenario and the use of time of the implantable devices. Besides, one of the severe restrictions in biomedical applications is the requirement that the maximum input power must be smaller than the upper bound of the human being safety, such as maximal Specific Absorption Rate (SAR), which disables the common WPT technologies to achieve their optimal efficiency operating conditions. In this chapter, an impulsive power transfer technologies with an impulsive generator circuit is demonstrated to receive sufficient external wireless power supply under low average input power (as illustrated in Figure 1) and convert the wireless power to the output voltage efficiently. We further design and implement an impulsive generator circuit to recharge the electronic devices wirelessly and compare with the traditional continuous wave techniques.

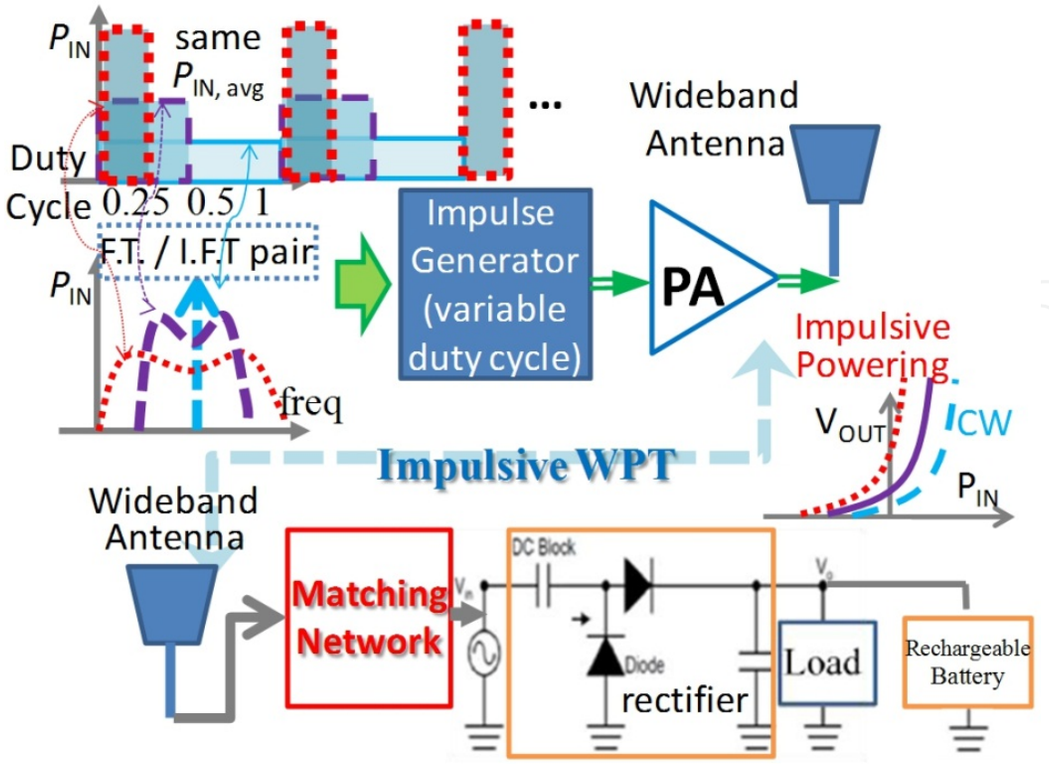

Figure 1. Schematic of proposed monocycle pulse generator.

To achieve the optimal conversion efficiency, proper operation condition should be well-controlled such as input power, resistive load, and loading currents to make proper matching network and optimize the rectifier efficiency [Yo 2008]. However, most of these circuits require driving at a high level of input power for its optimal efficiency, which is less preferred in biomedical applications due to the security concern, such as the regulations of SAR according to FCC or International Electrotechnical Commission (IEC). In this chapter, instead of using conventional CW for WPT, we further vary the duty cycles of the pulse waves and form a broadband power transmission system to promote the PCE of the rectifier at its weak power operation conditions.

Several wired and wireless experimental results prove that this technique is quite suitable for low input power transmission which is good for biomedical applications. In order to deliver the UWB power efficiently, a horn antenna with high directivity, large gain, and broad bandwidth acts as the transmit antenna. Also, biomedical environments are set to test the proposed system and a simplified wireless biomedical tissue model is assumed and analysed. The impulsive power generated by the impulse generator is amplified by the UWB power amplifier and then delivered through the horn antenna. The wideband power generated by the impulse generator is amplified by the UWB power amplifier and then delivered through the horn antenna. And the received impulsive power is converted into a direct current (dc) power by the Cockcroft–Walton type voltage-doubler rectifier composed of Schottky diodes to supply the chips or rechargeable batteries. In this chapter, the UWB impulsive wireless transmission systems have been proved to achieve 50% PCE even when the input power of the rectifier is lower than 0 dBm. Due to the fact that low transmission

power has relatively little impacts and causes relatively slight injury to human bodies, it is one of the essential key technologies in biomedical implant chips and devices.

2. System description of impulsive power transmission

The concept of the varying duty cycle is illustrated in Figure 1, and our testing system is shown in Figure 2. From Figure 1, we try to vary the duty cycle to form wideband power spectrum density (PSD) energy instead of conventional narrowband CW power. As the duty cycle reduces under the constraint of the same average input power, we observe that the output power of the rectifier increases dramatically according to the operation conditions such as pulse periods, resistance loading values, and channel conditions. The reason to gain much more efficiency will be addressed briefly in the following section.

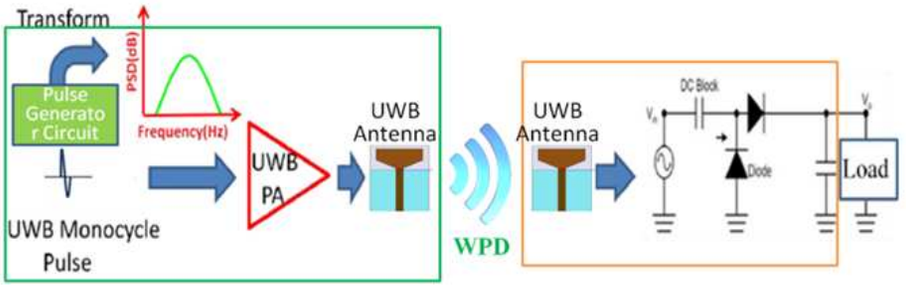

Figure 2. The testing system verifies the performance of impulsive wireless power transmission.

In Figure 2, a testing system to verify the output voltage and efficiency of impulsive powering is presented. This system includes an impulse generator circuit, a UWB PA, UWB antennas, and a two-stage rectifier to convert RF power into dc power. An UWB monocycle pulse generator is designed and fabricated by using both a shunt step recovery diode (SRD) and a wideband bipolar junction transistor (BJT), followed by a pulse shaping differentiator. This design will be presented and discussed in details later. The generator produces the extremely narrow impulse width about 290 ps, the ringing level is as low as -21.8 dB, and its measured bandwidth is 200 MHz to 6 GHz (5.8 GHz), whose circuit and performance will be addressed in Section 3. Then, we use an UWB PA to transmit the impulsive power through a pair of UWB antennas. The rectifier is a two-stage voltage doubler to convert the RF power to dc power. The rectifier can be high efficiency after an optimization procedure of careful design of the biasing of the input power and the resistive load, harmonic rejection, and the matching network [Yo 2004]. A similar rectifier circuit is used to examine the performance at a weak input power condition.

The concept of gaining extra output voltages can be explained from the non-linear transfer function of the rectifier which outputs more efficiently at high input power. Observing from the impulsive wave power distribution, the energy is concentrated within the specific pulse duration to enforce a high efficiency of the rectifier. When the pulse is off, the charged capacitor stored the energy and released with a relatively large time constant due to that the diodes are off and the reverse current is small. The analysis model of the PCE of the rectenna conversion efficiency depends on the diode electrical parameters and the circuit

losses at dc and the fundamental frequency. The mathematical model of the diode efficiency has been derived for varying input power levels [McSpadden 1998]. In this chapter, we try to build a probability model to evaluate the performance. The impulse power signal $V_{UWB}(t)$ generates a bi-state instant power distribution whose probability cumulative distribution functions (cdf) can be defined as $P_{cdf}(X) = Prob\{P_{instant\ (in\ dBm)} \leq X\}$.

$$P_{cdf,\ UWB}(X) = \begin{cases} 0 & X < 1 - D \\ P_{avg} / D & X \geq 1 - D \end{cases} \quad (1)$$

where X is the random variable of the instant powers in dBm and D is defined as the duty cycle for the impulse wave. Given the rectifier of the 2-stage voltage doubler follows a specific transfer function $V_{out}(t) = H_{rectifier}(P_{in,\ dBm}(t))$ at the moment t. This transfer function can be obtained by simulation with the (HSMS-286) Schottky diode precise models [Young 2002] or by measurement after well-matching. Because the exponential increase of the diode current with the growth of the input power biasing, the transfer function $H_{rectifier}(\cdot)$ is found to have the property of convex and increase monotonically and exponentially, which means the average over high $P_{cdf,\ UWB}$ will increase as the high instant P_{in} parts can be heavily weighted. Therefore, the average output voltage can be calculated as the expectation value of the input power according to the transfer function $H_{rectifier}(\cdot)$ and the probability distribution $P_{cdf,\ UWB}$ under the assumption that the Schottky diodes response quickly enough for these instant power variations of impulsive powers. The practical improvement ratios and trends can be estimated empirically varying with the different duty cycle D.

$$V_{out}(dc) = E\{ H_{rectifier}(P_{in,\ dBm})\} \quad (2)$$

From the experiments of impulsive tests, the output voltage increases significantly as duty cycle D decreases. Although at most of the time the instant power is zero, and yet a small portion of high peak power (P_{avg}/D) drives the rectifier with much higher efficiency under the exponential-like curve of $H_{rectifier}(\cdot)$. This implies that non-uniform power distributions can improve the output voltage by using some portion of large instance powers. For instance, the duty cycle reduces, and the instant power rises. Therefore, same average input power will result in higher PCE according to the portion of the high-level power and the peak values of the instant powers.

3. Circuit description and design

Pulse signals used in UWB systems are generally Gaussian pulses or monocycle pulses, both of which feature a wideband spectrum. The spectral characteristic of an ideal bipolar monocycle pulse do not include a dc component, and the frequency response is similar to that of a band pass filter. A spectrum with these characteristic provides a number of benefits for the wireless data transmission. Intuitively, an impulsive Gaussian wave can be generated by means of combining different phases Gaussian waves of different delay times. Then, a monocycle pulse is obtained by shaping the network and simple RC differentiator

[Reed 2005]. This is the principle on which pulse generators are generally based. Previous studies on UWB pulse generators are generally classified into four categories: logic gate-based pulses, modified oscillator- based designs [Teshirogi 2005], SRD-based generators as a waveform edge [Protiva 2010] sharpener, and transistor-based generators. In the past, monocycle pulse generators using SRD usually adopted serial connected prototypes, followed by a microstrip line stub with a shorted end.

In [Ma 2007][Han 2005], Han and Nguyen compared a shunt connected SRD with an inductor and serial connected SRD using a short circuited microstrip line stub. They demonstrated that a shunt SRD produces a pulse with less ringing [Ma 2007][Han 2005]. This makes a shunt-mode pulse generator a better choice for samplers. As suggested in [Ma 2007][Han 2005], we adopted a shunt SRD and second-order transient circuit to reduce ringing in our proposed pulse generator. Second-order RLC transient response was developed to produce a Gaussian pulse with reduced ringing, and BJT was used to perform impulse shaping to reduce ringing in the Gaussian wave even further [Han 2002]. For this reason, the monocycle pulse was created after the differentiator. The proposed device was fabricated using discrete components and a BJT. The fabricated pulse generator circuit demonstrated excellent performance in the aspects of pulse width, symmetry, and ringing.

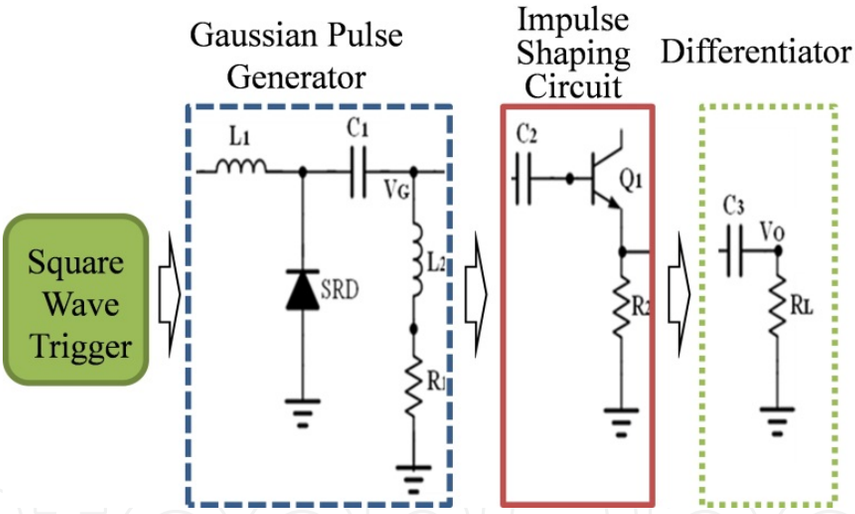

Figure 3. Schematic of proposed monocycle pulse generator.

As shown in Figure 3, the circuitry in the proposed monocycle pulse generator is laid out three parts: a Gaussian pulse generator, a pulse shaping circuit, and an RC differentiator. The Gaussian pulse is generated by the SRD accompanied by a second-order RLC transient circuit. Unlike pulses based on active transistors, the SRD requires no extra bias, and functions as a switch with extremely short transition time. The voltage across the serial inductor L_1 changes with the time-varying current through L_1. The voltage generates an instant, sharp spike at the moment that the shunt SRD switch turns off. The change in voltage on this serial inductor L_1 can be calculated from $V(t)=L_1 \, {}^{di(t)}/_{dt}$, where $i(t)$ is the current through L_1. Through the second-order transient circuit response of $R_1L_2C_1$, a sub-nanosecond Gaussian pulse can be created. According to Kirchhoff's rules, we obtain:

$$L_1 \frac{di(t)}{dt} = \frac{1}{C_1}\int i(t)dt + L_2 \frac{di(t)}{dt} + R_1 i(t) \tag{3}$$

Let $i(t) = k\, e^{st}$ and substitute it in (3), to obtain:

$$s = -\frac{R_1}{2(L_2-L_1)} \pm j\sqrt{\frac{1}{(L_2-L_1)C_1} - \left(\frac{R_1}{2(L_2-L_1)}\right)^2} \tag{4}$$

$$\equiv -\zeta \pm j\sqrt{w_o{}^2 - \zeta^2} = s_1, s_2 \tag{5}$$

where ω_o is the resonant frequency and ζ is the damping coefficient. The solution is:

$$i(t) = k_1 e^{-s_1 t} + k_2 e^{-s_2 t} \tag{6}$$

According to (5), a change in damping coefficient ζ can be classified according to three types of second-order transient responses: under-damping ($\zeta<\omega_o$), critical-damping ($\zeta=\omega_o$), and over-damping ($\zeta>\omega_o$). To reduce ringing in the monocycle pulse, the over-damping transient condition was selected as the principle component in the design of the Gaussian pulse (on node V_G). A wideband BJT (Q_1) and simple RC differentiator were used to convert the Gaussian pulse into a bipolar monocycle pulse. A passive wideband BJT (Q_1) was intentionally selected to function as a diode (base-emitter junction) in shaping Gaussian pulses. Additional DC offset is not required due to that the shallow emitter and the narrow base width, a fast transitional behavior of this wideband BJT which operates in the diode mode can be achieved, so a fast transition can be available by using this EB junction diode.

When the Gaussian pulse is on the rising edge, the BJT (Q_1), functioning as a diode, turns on to charge the capacitor C_3. Conversely, when the Gaussian pulse is on the falling edge, the capacitor C_3 provides a reverse bias to the BJT (Q_1) to shut down Q_1 and discharges through R_2. The width of the Gaussian pulse can be further compressed after shaping. Finally, the Gaussian pulse is differentiated into a monocycle pulse through a simple RC differentiator. The simulation results of Gaussian pulse and monocycle pulse waveforms are shown in Figure 4. A pulse width of 280 ps was generated; however, the amplitude was reduced considerably from 1.25V to 0.235V, due to loss in the differentiator. Figure 4(b) is the Fourier transform of the simulated pulse in the frequency domain, implying an ultra-wide bandwidth of nearly 5.7 GHz (220 MHz–5.9 GHz). According to the simulation, the ringing ratio can be further reduced by exploiting its symmetrical waveform. Ringing exists in all practical impulse circuits; however, compensation can be used to reduce the effects of ringing. If positive and negative cycles have precisely the same pulse width and opposite phase ripple, then the ringing can be reduced to the minimal level. Ringing is optimized according to the second-order transient response, the shaping network, and RC differentiator. However, this monocycle pulse still encounters ringing, due mainly to the unbalanced switching transient time of BJT (Q_1), noise from fabrication, and tolerances of the component values.

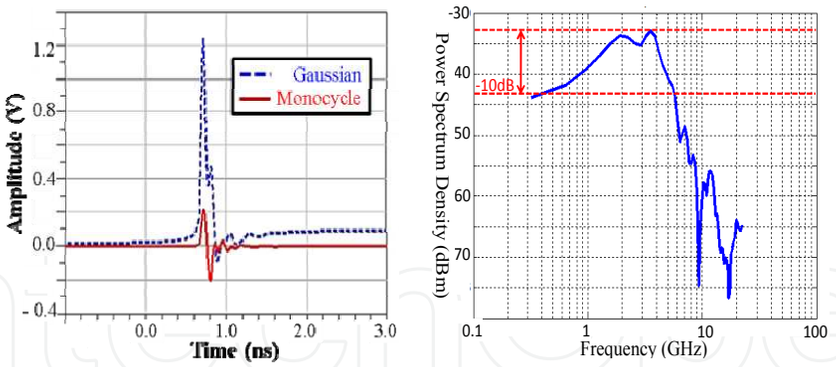

Figure 4. (a) Simulated waveforms of the Gaussian pulse and monocycle pulse using over-damping response in time domain; (b) The spectrum of the simulated monocycle pulse.

4. Wireless channel model through tissues

A RF-DC rectifier circuit is one of the core techniques in microwave wireless power transmission. Moreover, the PCE is the major parameter for the performance of the rectifier circuit [Yoo 1992]. To achieve the optimal PCE, the wireless power systems need to operate with proper loads and at high input power. However, when such techniques are practically applied in biomedical purposes or implanting systems, there are many limitations such as SAR regulations, the limited space, biomedical compatibility, the transmission distance, and the absorption of the human beings' tissues. Mostly, the received power is very weak in such wireless power transmission applications, so the rectifier cannot achieve high Vout and good PCE. Therefore, it is a crucial issue of promoting the V_{out} and PCE of rectifier at low input power level under a proper consideration of the tissue effects.

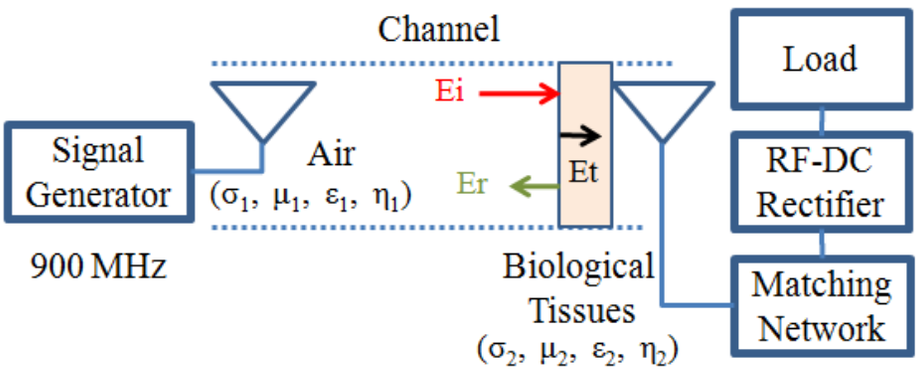

Figure 5. System block diagram of wireless power transmission.

For the applications of the wireless power transmission in practical biomedical environments, it is inevitable to deal with many loss factors in wireless channels. In addition to the factors of the free-space path loss (FSPL), standing waves, polarization mismatch of the microwave power, the attenuation in the wireless channels becomes much more complicated under the influences of the biological tissues such as muscle, bone, and fat dielectrics which produces different biological attenuation and the reflection between the

interface. This chapter provides a novel technique to improve the V_{out} and PCE at low input power level (P_{IN}). We also built up analysis models and design the experiments of the power transmission over different media channels of wired transmission, air transmission and the biological tissues to validate the impulsive wireless power transmission techniques. The influence from the biological tissues is also another main concerned factor in wireless power transmission to address in this chapter.

5. Channel model

The channel model of the wireless power transfer system is simply shown in Figure 5. Due to the complexity of the realistic wireless transmission channel, we will create a simple model in this chapter to simplify the loss from the transmission channel without the complicated multipath influences and fading phenomenon. We assume the biological tissues to be muscles, and the main factors of attenuation are considered including FSPL (L_{path}), biological tissue loss (L_{tissue}), and the reflection loss ($L_{interface}$) over the interface. We can establish the fundamental analysis to estimate the loss of transmission channel as the equations below.

We assume the antenna gain is 0 dBi and the microwave transfers in free space without obstacles nearby to cause reflection or diffraction, so we may apply Friis Formula to estimate the path loss. From (7), we found that as the wavelength decreases, FSPL will increase significantly. The numerical results are shown as Figure 6(a).

$$\text{FSPL} = (\frac{4\pi d}{\lambda})^2 = L_{\text{path}} \tag{7}$$

where d is the distance between the transmitter and receiver and λ is the wavelength.

We assume the tested muscle as a homogeneous medium. From (8) and (9), the biological tissue loss is determined by the propagation constant and the thickness of tissue. From (10), the propagation constant is determined by frequency, σ, μ, and ε of the tissue [Gabriel 1996]. So the biological tissue loss increases as the frequency or the thickness of the tissue increases. The related equations can be analyzed as below.

$$E_x = E_0 e^{-\alpha z} \tag{8}$$

$$L_{\text{tissue}} = \frac{E_0 - E_x}{E_0} = 1 - e^{-\alpha z} \tag{9}$$

$$\alpha = R_e(\gamma)\ ,\ \gamma = j\omega\sqrt{\mu\varepsilon}\sqrt{1 - j\frac{\sigma}{\omega\varepsilon}} \tag{10}$$

where σ : conductivity, γ : propagation constant

$$\mu = \mu_0\mu_r : \text{permeability},\ \varepsilon = \varepsilon_0\varepsilon_r : \text{permittivity}$$

Microwave power of different frequencies pass through the media with the different intrinsic impedances causes the different amount of the incident power and reflected power.

This can be calculated by (11). The reflected power tends to decrease as the frequency increases, and it does not vary as much after the frequency is higher than 400 MHz (as shown in Figure 6 (a)).

$$L_{\text{interface}} = \Gamma =, \frac{E_r}{E_i} = \frac{\eta_2 - \eta_1}{\eta_2 + \eta_1}, \ \eta = \sqrt{\frac{j\omega\mu}{\sigma + j\omega\varepsilon}} \tag{11}$$

where η : intrinsic impedance

Let the distance of the transmitter and the receiver be 60 cm and thickness of the pork be 1 cm. The losses of the wireless channel are mainly composed of L_{path}, L_{tissue}, and $L_{interface}$. When one of them increases greatly, the channel loss will also increase dramatically. As the Figure 6(a) shows, when the frequency increases, the overall channel loss increases substantially due to the significant increase of FSPL. As the frequency and tissue thickness increase, the loss of biological tissues increases as Figure 6(b) below.

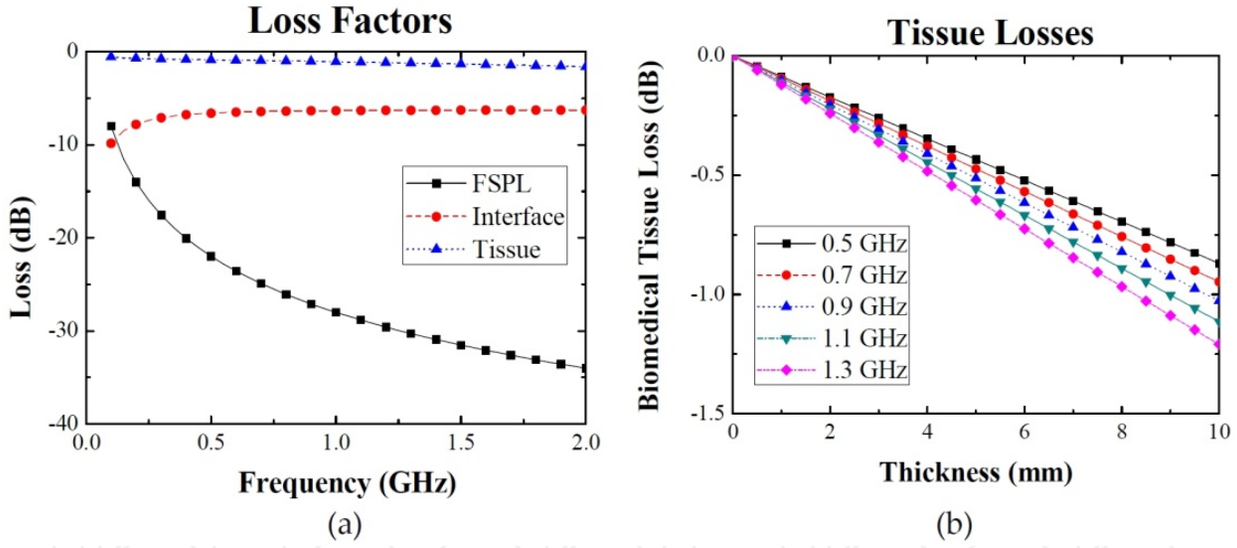

Figure 6. (a) The losses in different frequencies; (b) The biomedical tissue loss of different thickness.

To deal with detailed E and H-fields, Poynting vector can be obtained as follows.

$$\begin{aligned} \bar{H}^i &= \sqrt{\frac{j\omega\mu_0\left(j\omega\varepsilon_{1(air)} + \sigma_{1(air)}\right)}{\left(j\omega\mu_0\right)^2}} E_0 e^{-\gamma_{1(air)}z}\hat{y} \\ &= \sqrt{\frac{j\omega\varepsilon_{1(air)} + \sigma_{1(air)}}{j\omega\mu_0}} E_0 e^{-\gamma_{1(air)}z}\hat{y} \end{aligned} \tag{12}$$

The incident wave's H-field ($\bar{H}^i$), the reflection ($\bar{H}^r$), and transmissionas ($\bar{H}^t$) can be expressed as a function of the wave impedance:

$$\vec{H}^i = \hat{y}\frac{E_0}{\eta_{1(air)}}e^{-\gamma_{1(air)}z} \tag{13}$$

$$\vec{H}^r = -\hat{y}\frac{RE_0}{\eta_{1(air)}}e^{-\gamma_{1(air)}z} \quad , \quad \vec{H}^t = \hat{y}\frac{TE_0}{\eta_{2(skin)}}e^{-\gamma_{2(skin)}z} \tag{14}$$

where the transmission coefficients is obtained by

$$T = \frac{2\eta_{2(skin)}}{\eta_{2(skin)} + \eta_{1(air)}} \tag{15}$$

Last, the Poynting vector, which represents the power density in W/m^2, is given by

$$\vec{S} = \vec{E} \times \vec{H} \Rightarrow |S| = |E||H| \tag{16}$$

Therefore, the incident and reflection power densities at the interface on the air-side and the transmission power density at the interface on the skin-side are:

$$\left|S_{1(air)}{}^i\right| = \frac{E_0{}^2}{\eta_{1(air)}}, \qquad \left|S_{1(air)}{}^r\right| = \frac{\Gamma^2 E_0{}^2}{\eta_{1(air)}}, \qquad S_{2(skin)}{}^t = \frac{T^2 E_0{}^2}{\eta_{2(skin)}} \tag{17}$$

Finally, the ratios of transmission-to-incident power ($P_{t/i}$) and reflection-to-incident power ($P_{r/i}$) are:

$$P_{r/i} = \frac{\left|S_{1(air)}{}^r\right|}{\left|S_{1(air)}{}^i\right|} = \Gamma^2, \qquad P_{t/i} = \frac{\left|S_{2(skin)}{}^t\right|}{\left|S_{1(air)}{}^i\right|} = \frac{T^2 \eta_{1(air)}}{\eta_{2(skin)}} \tag{18}$$

6. Fabrication and measurement setup

The impulsive wave is amplified with an UWB PA (ZRON-8G) whose bandwidth is 2-8 GHz and its gain is almost constantly 20 dB over this band. Then the power is transmitted and received with a pair of UWB horn whose gain is 10 dBi. The received power is fed into a two-stage voltage doubler as shown in Figure 7. C_1 (0.1 pF) is used to filter out the dc component and C_2 (1 pF) functions as the ripple and noise filter. The rectifier usually requires to be optimized according to its input power biasing and the resistive load value. However, it is not easy to match to our UWB pulse signals up to 5.8 GHz, so we simply apply the broadband feature of the Schottky diodes to transfer the broadband power, yet this system is not optimal at this stage. The whole receiving circuit is fabricated on the substrate of Rogers RO4003C. We will compare two major performance parameters. One is the conversion efficiency and we try to figure out the optimal operation condition for an UWB powering transmission system. The other is to compare the difference of the input power of the rectifier to generate the same output voltage. That is useful to count how much power is saving for the same output voltage level.

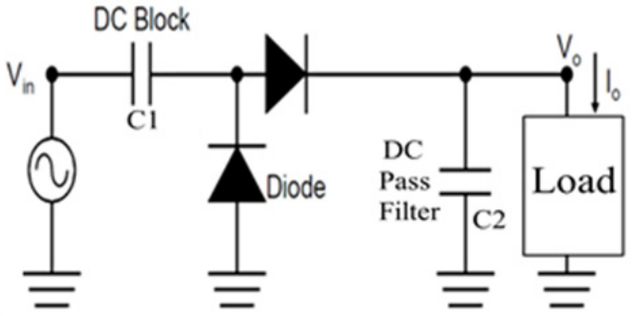

Figure 7. The circuit of the voltage doubler for the testing system of impulsive wireless power transmission.

A prototype of this monocycle pulse generator was implemented using discrete components. The substrate of the high frequency circuit was Rogers RO4003C with the dielectric constant of 3.55 and thickness of 32 mil (0.8182 mm). MuRata surface mount devices (SMD) and discrete components of the pulse generator are listed below. The optimized values of the components were L_1=3 nH, L_2=4.7 nH, C_1=C_2=3 pF, and R_1=R_2=150 Ω, based on theoretic simulations and fine tuning in the fabrication process. The driving inductance L_1 of the second-order transient circuit was estimated for the initial design using the equations in [Han 2005], and 3 nH, L_2, and R_1 were selected to ensure over-damping conditions according to the analysis in Section 3. However, the combination of C_1 and the equivalent resistance, R_{eq}, of R_1 and impedance of the BJT resulted in a high-pass filter for the input driving signal. Therefore, C_1 may be too small, blocking the generated pulses. In addition, the upper bound of C_1 can be estimated by preventing the input clock signal, with a rise time of t_r, from slewing; thereby implying $C_1 < t_r / (2.2R_{eq})$. C_2 was used to remove the dc component of the impulse and had to be kept small in consideration of the total equivalent capacitance value. Finally, R_2 and C_3 were fine tuned in ADS simulation to produce a symmetrical waveform. BFG520 BJT (Philips Semiconductor, NXP) was selected for its wideband, extending up to 9 GHz. Metelics MMDB30-0805 SRD with 0.46 pF junction capacitance provided an extremely short transition time of 30 ps.

A testing system of impulsive wireless power transmission is setup to measure its power conversion efficiency and to compare with the traditionally continuous wave WPT systems. The impulse generator is triggered with a 10 MHz square wave with amplitudes of 2, 3, 4, and 5 Vpp, and the generator outputs average power (instant peak power) of -31.0 dBm (2.83 dBm), -27.3 dBm (7.14 dBm), -25.1 dBm (10.10 dBm), and -23.7 dBm (11.86 dBm), respectively. The power is calculated according to equation (19):

$$P_{UWB,\,avg} = \text{The power of a mono} - \text{pulse / The period of trigger signals} \quad (19)$$

7. Results and discussion

7.1. Waveform of pulse generator circuit

Figure 8 presents the results of characterizing the waveform of the monocycle pulse. Figure 8(b) is the Fourier Transform of the measured pulse in the frequency domain, implying an ultra-

wide bandwidth of 5.2 GHz (900 MHz – 5.1 GHz). The measured and simulated results were closely matched. The width of the output pulse of the generator circuit was approximately 290 ps, and the amplitude was 310 mV (peak-to-peak). The symmetry is evident in the similarities in amplitude and width in the positive and negative cycles of the measured waveform. The monocycle pulse has a highly symmetrical shape. Conversely, when the positive and negative cycles differ in amplitude and width, the pulse width cannot be minimized and the sidelobe ringing increases. This can be dealt with by carefully tuning the differentiator circuit during fabrication. Moreover, this aspect of symmetry can reduce the ringing even further. In the end, the ringing level was reduced to only -21.8 dB. Ringing level is defined as

$$20\log\left[\frac{\text{The peak-to-peak value of ringing}}{\text{The peak-to-peak value of monocycle pulse}}\right] \quad (20)$$

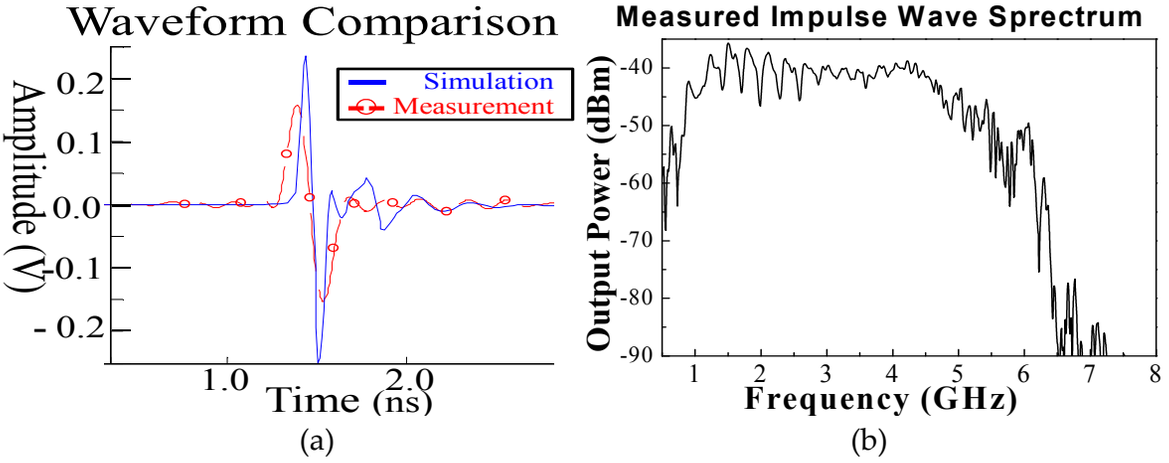

Figure 8. (a) Comparison of simulated and measured pulse waveforms; (b) Response of the measured monocycle pulse in frequency domain.

Unlike some generators requiring high frequency sources, we used a 10-MHz or lower square wave signal as a trigger source, applying a high speed digital real-time oscilloscope (Agilent DSO81204B) to measure the pulse in the time domain. Moreover, the frequency range of the input triggered square waves can be very broad. In this study the range was verified to cover 30 Hz to 30 MHz, resulting in stable monocycle pulse waveforms of identical widths with variations in the amplitude of less than 3 %. This implies that a triggering square wave circuit can be simple and does not require a specific frequency range, eliminating the need for a bulky external signal generator.

Figure 9 presents the results of measuring the monocycle pulse waveform using a triggering source of 10 MHz square waves with amplitudes of 2 to 5 V. When the amplitude of the triggering source was increased, the amplitude of the monocycle pulse also increased. The width of the pulse remained unchanged, as shown in Figure 9. The ringing ratio was not amplified, but remained below -21 dB. Maintaining ultra low ringing is beneficial to UWB communication systems. Details of the monocycle pulse are summarized in Table 1. Positive and negative cycles are nearly equal in amplitude and duration, demonstrating a high degree of symmetry.

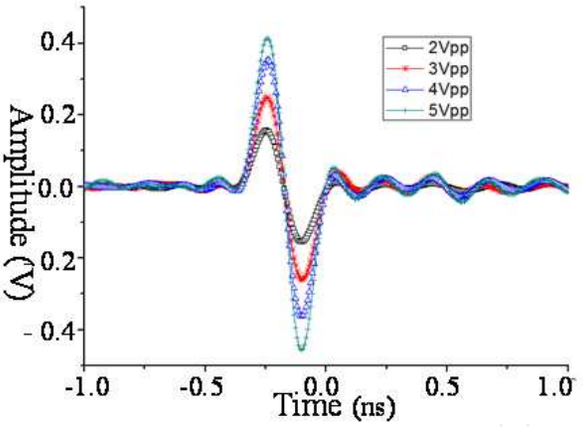

Figure 9. Measurement results with variations in triggering amplitude.

Trigger Square Wave Amplitude (V_{pp})	Output Peak-to-peak Amplitude (mV)	Ringing Level (dB)
2	320.0	-21.8
3	509.0	-21.0
4	716.0	-21.5
5	876.0	-22.0

Table 1. Monocycle Pulse in Relation to Triggering Amplitudes

Table 2 provides a comparison of performance between various monocycle pulse generators fabricated with discrete components that have appeared in recent publications. Each of these devices generates sub-nanosecond pulse waveforms with additional dc bias; however, our proposed hybrid shunt SRD and BJT pulse shaping circuitry requires no dc bias. Moreover, as seen in this table, our design has the advantage of tunable pulse amplitude, ultra low ringing, short pulse width, and excellent symmetry.

Reference	[Han 2002]	[Lee 2001]	[Miao2006]	**This work**
Peak-to-peak Amplitude (mV)	400	700	300~600	**320 ~ 876**
Ringing Level (dB)	-17	-20.9	-16.9 ~ -16	**-21.8**
Pulse Duration (ps)	300	350	200 ~ 400	**290**
Technology	SRD	SRD	CMOS	**SRD/BJT**

Table 2. Comparison of This Work to Other Pulse Generators

7.2. Wired transmission verification

We observe the impacts of reducing duty cycles of the impulse waves under same average input power (-10 dBm) on the PCE through a short low loss coaxial cable to remove the wireless channel uncertainties. As the duty cycles reduce, the larger instant power helps to overcome the potential barrier of the rectifier circuits, so the PCE can be improved. However, on the other hand, the wider bandwidth of matching network is required and parts of the power are out of band, so the PCE cannot achieve to its maximum as the duty cycles becomes smaller and smaller. The measured results are shown in Figure 10.

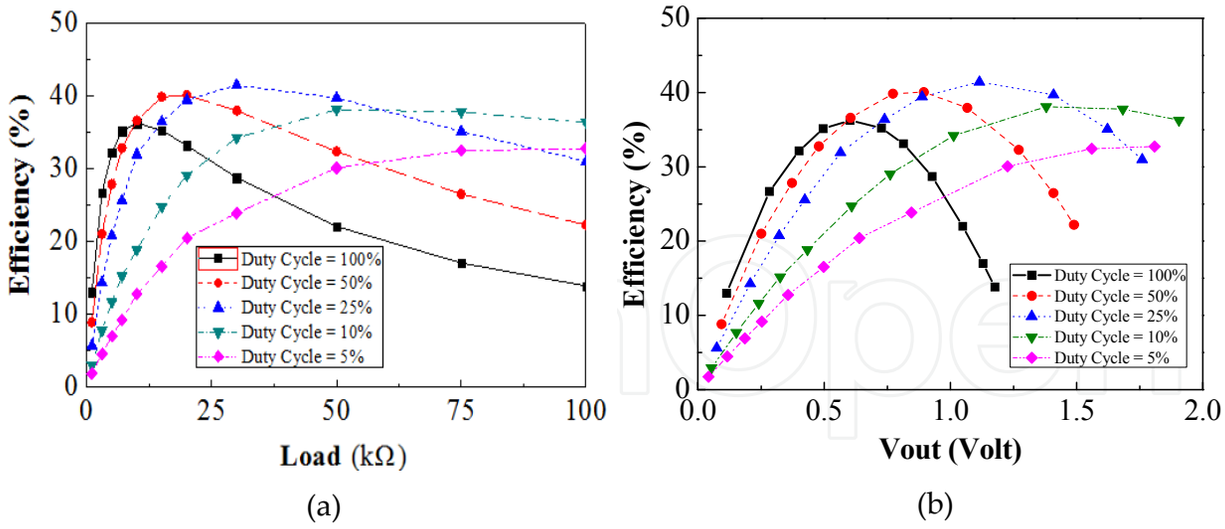

Figure 10. (a) The efficiency of different duty cycles and different resistive load under the same average input power. (b) The efficiency of different duty cycles and different Vout under the same average input power.

As the Figure 10(a) shows, the optimal PCE can be achieved when the load is 30 kΩ and the duty cycle is 25%. After that, even though the duty cycle reduces, the PCE starts to decrease instead. Given a 100 kΩ, the maximal PCE can be improved by 22.46% and this is almost twice efficient as the original CW power transmission (16%). The PCE can be ranked in the duty cycles of 10%> 5%> 25%> 50%> 100%. The best PCE can be achieved at duty cycle 10%, not 5%. As the Figure 10(b) shows, the output voltage V_{out} is raised from 1.176 to 1.905 volt. Therefore, one more dimension of freedom is created to meet the optimal PCE and the required V_{out} by varying the duty cycles under specific loading.

7.3. The input power gain to obtain same output voltage

To compare the performance of our fabricated impulsive generator for WPT, the circuit is triggered with a 10-MHz square wave from 2 Vpp to 5 Vpp and produces the impulsive power (after a 20 dB PA) from -11 dBm to -3.7 dBm. The output voltages are recorded, and the traditional CW which is optimized reproduces this same output voltage level. The difference of the input power is called saved input power, which implies a better efficiency of the rectifier to output same voltage with less average input power. The results are shown in Table 3. The saved input power of the impulsive powering systems ranges from 1.6 dB to 2.1 dB, which is a worse case. When the trigger source is replaced with a 40 MHz one, the saved input power ranges from 8.4 dB to 10.6 dB.

7.4. The optimal Power Conversion Efficiency (PCE)

The fabricated impulsive generator is applied as the power source with the different trigger signals ranging from 10 MHz to 40 MHz to output the different power level ranging from -11 dBm to 13.6 dBm after some adjustment of a -10 dB attenuator and a 20-

dB PA. The output voltage with the 30 kΩ resistive load is shown in Figure 11. We found the P_{IN} for optimal PCE (58%) operation reduces to -2.4 dBm. Compared with traditional CW WPT techniques, high efficiency may be achieved under the operation condition of P_{IN} > 7.5 dBm. This validates our assumption to apply such wideband powering techniques for low input power to generate high output voltage and to enhance the conversion more efficiently.

To Obtain Same V_{out} (V)	Input Power Required by		Input Power Saving Ratio (dB)
	Using Impulse (dBm)	Using CW (dBm)	
0.700	-11.0	-8.9	2.1
1.207	-7.3	-5.5	1.8
1.601	-5.1	-3.4	1.7
1.900	-3.7	-2.1	1.6

Table 3. The comparison of the input power between impulsive (triggered with a 10 MHz source) and CW with a 12 kΩ load

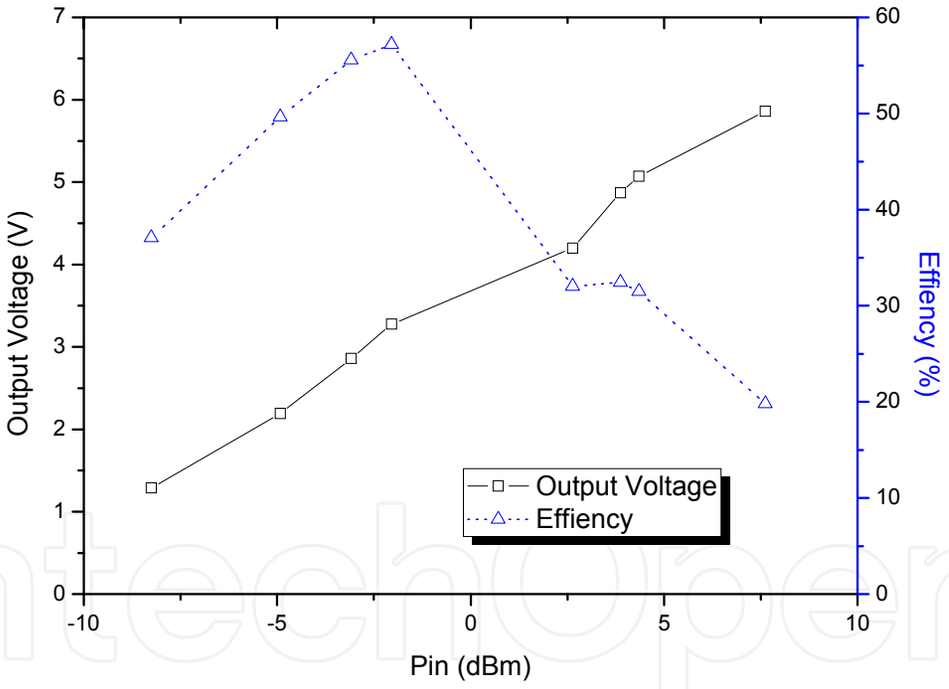

Figure 11. The performance of the wideband rechanging for the resistive load of 30 kΩ.

7.5. The impulse wireless powering transmission

Last, the impulsive wireless power transmission tests at a distance of 50 cm and 60 cm are performed. The impulsive generator is triggered at 40 MHz square waves and outputs power ranging from -4.8 dBm to 3.9 dBm. The transmission and receipt antennas are using horn antennas of 10 dBi. The results are shown in Table 4. Due to the path loss attenuation, the output voltages are low but are still good for circuits of low power supply of 1.2 V.

Impulsive Power Trigger with 40 MHz + 20-dB PA (dBm)	V_{out} at Distance of 50 cm (V)	V_{out} at Distance of 60 cm (V)
-4.8	0.336	0.262
-0.8	0.730	0.611
1.7	1.060	0.910
3.9	1.250	1.100

Table 4. The performance of output voltage using impulsive wireless power transmission with horn antennas

8. Conclusion

In this chapter, a novel impulsive UWB technology is proposed for wireless power transmission, and we designed, fabricated, and validated an improved UWB monocycle pulse generator using a hybrid shunt SRD and wideband BJT. Applying a shunt SRD with a second-order circuit produces a sharp Gaussian pulse, the waveform of which can be converted into monocycle impulse signals after the wideband BJT and RC differentiator. Measurement results closely match those of simulation. The fabricated monocycle pulse generator outputs a symmetrical 290 ps impulse with extremely low ringing (-21.8 dB) triggered by a square wave source across a wide frequency range of 30 Hz to 30 MHz. The proposed impulse generator circuit is well suited to UWB applications with the advantages of simple design, low cost, highly symmetrical impulses, and low ringing.

This novel impulsive generator is applied for wideband wireless power transmission and is verified in experiments. An impulsive generator is designed and fabricated as the experimental testing sources. The measurement results show that the PCE can achieve 50% efficiency by applying the impulsive WPT when the average input power remains below 0 dBm. This novel concept opens a broad angle for the future research of wireless power transmission technologies. In the future, wireless power transmission technologies can be developed in diversifed methods such as wideband power or multiple CW powers.

Author details

Chin-Lung Yang, Yu-Lin Yang and Chun-Chih Lo
Department of Electrical Engineering, National Cheng Kung University, Tainan, Taiwan (R.O.C.)

9. References

Bertoni, H. L.; Carin, L.; Felsen, L. B. (1992). *Ultra-wide band short pulse electromagnetic*, New York, Kluwer Publications, (1992).

Brown, W. C.; Mims, J. R.; Heenan, N. I. (1965). An Experiemental Microwave-powered Helicopter, *IRE International Convention Record*, vol. 13, part 5, (Mar. 1965) , pp. 225-235.

Gabriel, S.; Lau, R.W.; Gabriel, C. (1996). The Dielectric Properties of Biological Tissues: III Parametric Models for The Dielectric Spectrum of Tissues, *Physics in Medicine & Biology*., vol. 41, (1996), pp. 2271–2293.

Han, J.; Nguyen, C. (2002). A new ultra-wideband, ultra-short monocycle pulse generator with reduced ringing, *IEEE Microwave Wireless Compon Lett*, 12 (2002), 206-208.

Han, J.; Nguyen, C. (2005). Coupled-slotline-hybrid sampling mixer integrated with step-recovery-diode pulse generator for UWB applications, *IEEE Trans Microwave Theory Tech*, 53 (2005), 1875-1882.

Hirt, W. (2003). Ultra-wideband radio technology: Overview and future research, *Computer Commun J*. 26 (2003), 46–52.

Kurs, A.; Karalis, A.; Moffatt, R.; Joannopoulos, J. D.; Fisher, P.; Soljačić, M. (2007). Supporting Online Material for Wireless Power Transfer via Strongly Coupled Magnetic Resonances, *Science Magazine*, (June 2007).

Lee, J. S.; Nguyen, C.; Scullion, T. (2001). New uniplanar subnanosecond monocycle pulse generator and transformer for time-domain microwave, *IEEE Trans Microwave Theory Tech*, 49 (2001), 1126-1129.

Ma, T.-G.; Wu, C.-J.; Cheng, P.-K.; Chou, C.-F. (2007). Ultrawideband monocycle pulse generator with dual resistive loaded shunt stubs, *Microwave Opt Technol Lett 23* (2007), 459–462.

McSpadden, J.O.; Lu, F.; Chang, K. (1998). Design and Experiments of a High Conversion Efficiency 5.8-GHz Rectenna, *IEEE Transactions on Microwave Theory and Techniques*, vol. 46, (Dec. 1998), pp.2053-2060.

Miao, M.; Nguyen, C. (2006). On the development of an integrated CMOS-based UWB tunable-pulse transmit module, *IEEE Trans Microwave Theory Tech*, 54 (2006), 3681–3687.

Protiva, P.; Mrkvica, J.; Macháč, J. (2010). A compact step recovery diode subnanosecond pulse generator, *Microwave Opt Technol Lett 52* (2010), Iss.2, 438-440.

Reed, J. H. (2005). *An introduction to ultra wideband communication systems*, Prentice Hall PTR, (2005).

Rodenbeck, C.; Li, M.; Chang, K. (2004). A Phased-array Architecture for Retrodirective Microwave Power Transmission from the Space Solar Power Satellite, *IEEE MTT-S International Microwave Symposium Digest*, vol. 3, (June 2004), pp.1679-1682.

Teshirogi, T.; Saito, S.; Uchino, M.; Ejima, M.; Hamaguchi, K.; Ogawa, H.; Kohno, R. (2005). Residual-carrier-free burst oscillator for automotive UWB radar applications, *Electron Lett* 41 (2005), 535–536.

Yang, C.-L.; Lo, C.-C.; Yang, Y.-L. (2003). Sub-nanosecond Pulse Generators for Impulsive Wireless Power Transmission, *IEEE Transactions on Circuits and Systems II*, (Dec. 2011), pp. 817 - 821.

Yo, T.-C.; Lee, C.-M.; Hsu, C.-M.; Luo, C.-H. (2008). Compact Circularly Polarized Rectenna with Unbalanced Circular Slots, *IEEE Transactions on Antenna and Propagation,* (Mar. 2008), vol. 56, no. 3, pp. 852-886.

Yoo. T.; Chang, K. (1992). Theoretical and Experimental Development of 10 and 35 GHz Rectennas, *IEEE Transactions on Microwave Theory and Techniques*, vol. 40, no. 6, (Jun. 1992), pp.1259-1266.

Young, H. S.; Chang, K. (2002). A High Efficiency Dual Frequency Rectenna for 2.45- and 5.8-GHz Wireless Power Transmission, *IEEE Transactions on Microwave Theory and Techniques*, vol. 50, (July 2002), pp.1784-1789.

Zimmerman, M.; Chaimanonart, D.N.; Young, D. J. (2006). *In Vivo* RF Powering for Advanced Biological Research, *Engineering in Medicine and Biology Society, EMBS 28th Annual International Conference of the IEEE*, (2006), pp. 2506-2509.